

# Noninvasive laser-induced photoacoustic tomography for structural and functional *in vivo* imaging of the brain

Xueding Wang<sup>1</sup>, Yongjiang Pang<sup>1</sup>, Geng Ku<sup>1</sup>, Xueyi Xie<sup>1</sup>, George Stoica<sup>2</sup>, & Lihong V Wang<sup>1</sup>

Imaging techniques based on optical contrast analysis can be used to visualize dynamic and functional properties of the nervous system via optical signals resulting from changes in blood volume, oxygen consumption and cellular swelling associated with brain physiology and pathology. Here we report *in vivo* noninvasive transdermal and transcranial imaging of the structure and function of rat brains by means of laser-induced photoacoustic tomography (PAT). The advantage of PAT over pure optical imaging is that it retains intrinsic optical contrast characteristics while taking advantage of the diffraction-limited high spatial resolution of ultrasound. We accurately mapped rat brain structures, with and without lesions, and functional cerebral hemodynamic changes in cortical blood vessels around the whisker-barrel cortex in response to whisker stimulation. We also imaged hyperoxia- and hypoxia-induced cerebral hemodynamic changes. This neuroimaging modality holds promise for applications in neurophysiology, neuropathology and neurotherapy.

Further functional imaging techniques other than functional magnetic resonance imaging (fMRI) and positron emission tomography (PET) are needed to advance the field of neuroscience. Optical imaging of the brain is highly desirable because it is a functional approach<sup>1–5</sup>. Its advantage over fMRI is that optical contrast can be used to assess simultaneously both oxy- and deoxyhemoglobin<sup>6,7</sup> and can also detect intracellular events related to neuronal activities with a fast and direct response to stimulation<sup>2,8</sup>. Pure optical imaging, however, has significant drawbacks: transcranial imaging has poor spatial resolution as a result of the overwhelming scattering of light in biological tissues<sup>8</sup>, and invasive open-skull imaging has no depth resolution<sup>9–12</sup>.

Photoacoustic tomography (PAT) in biological tissues<sup>13–19</sup> overcomes the resolution disadvantages of pure optical imaging and the contrast and speckle disadvantages of pure ultrasonic imaging<sup>20</sup>. Here we report the development of a PAT technique, based on contrasts in optical absorption (also called optical energy deposition), for functional imaging of the brains of small animals *in vivo*. We used this to visualize brain structure, brain lesions, cerebral hemodynamic responses to hyperoxia and hypoxia, and cerebral cortical responses to neural activities induced by whisker stimulation in rats. We show that (i) structural PAT of soft tissues, including lesions in the rat brain, provides high intrinsic contrast, (ii) functional PAT based on intrinsic optical signals can be used to map the functional organization of the cerebral cortex and (iii) in contrast to earlier optical methods, this technique allows completely noninvasive transdermal and transcranial neuroimaging at high spatial resolution with the skin and skull intact.

## RESULTS

### PAT system for noninvasive imaging of the rat brain *in vivo*

To produce photoacoustic waves—based on laser-induced thermoelastic expansion<sup>21,22</sup>—efficiently in biological tissues, a short laser

pulse is required. A Q-switched Nd:YAG laser (Fig. 1) was adopted to provide 532-nm laser pulses with a full-width half-maximum (FWHM) value of 6.5 ns. The laser beam was expanded and homogenized to provide an incident energy density of <10 mJ/cm<sup>2</sup> on the skin of the rat head, which induced an estimated <20 mK temperature increase in the skin. The distribution of optical absorption in the brain tissues generated proportionate photoacoustic waves, which were coupled into a high-sensitivity, wide-bandwidth (88% at –6 dB with a center frequency of 3.5 MHz) ultrasonic transducer (V383, Panametrics) through the water in the assay tank. The transducer, driven by a computer-controlled step motor to scan around the rat head, detected the photoacoustic signals in the imaging plane at each scanning position. The transducer was cylindrically focused with a focal diameter of ~1 mm, which determines the spatial resolution along the *z*-axis. A pulse amplifier (500 PR, Panametrics) received the signals from the transducer and delivered the amplified signals to a digital oscilloscope. Finally, a computer collected the digitized photoacoustic signals to reconstruct the distribution of optical absorption within the sample<sup>23</sup>, which determines the resolution in the *x-y* imaging plane.

### Image reconstruction

For the photoacoustic effect in our system, heat conduction can be neglected because the duration of the laser pulse is much shorter than the thermal diffusion time<sup>21</sup>. Our recent development of an accurate reconstruction algorithm<sup>23</sup>, and the configuration of the laser illumination relative to the acoustic detection plane in combination with full-view detection of the imaging cross-section, were crucial elements in the development of our approach. For cases where the scanning radius in a circular scan configuration is much greater than the photoacoustic wavelengths (which was true in our

<sup>1</sup>Optical Imaging Laboratory, Department of Biomedical Engineering, and <sup>2</sup>Department of Pathobiology, Texas A&M University, College Station, Texas 77843-3120, USA. Correspondence should be addressed to Lihong V. Wang (lwang@tamu.edu).

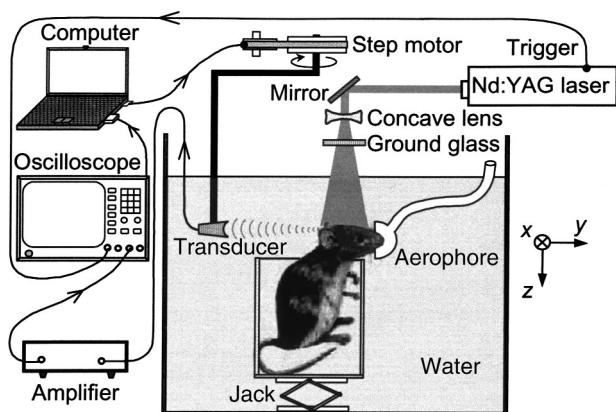


**Figure 1** PAT setup for noninvasive transdermal and transcranial imaging of the rat brain *in vivo* with the skin and skull intact.

experiments), the optical absorption,  $A(\mathbf{r})$ , within the sample at a given position  $\mathbf{r}$  is

$$A(\mathbf{r}) = -\frac{r_0^2 C_p}{2\pi v_s^4 \beta} \int_{\theta_0} d\theta_0 \frac{1}{t} \frac{\partial p(\mathbf{r}_0, t)}{\partial t} \Big|_{t=|r_0-\mathbf{r}|/v_s} \quad (1)$$

where  $C_p$  is the specific heat,  $v_s$  is the acoustic speed,  $\beta$  is the thermal coefficient of volume expansion,  $r_0$  is the detector position with respect to the imaging center and  $p(\mathbf{r}_0, t)$  is the photoacoustic signals detected at each scanning angle  $\theta_0$ .

### Structural imaging and lesion detection

The noninvasive transdermal and transcranial image of the superficial layer of the rats' brains *in vivo* (Fig. 2a) matched well with an anatomical photograph obtained after imaging (Fig. 2b). Owing to their different optical absorptions, various soft tissues in the brain were clearly identifiable. A large contrast in optical absorption was visible between blood vessels and the background parenchyma, ranging from 2.3 to 7.9. A rat with a superficial lesion in the right cerebral cortex was also imaged by our PAT system with the skin and skull intact. The position and shape of the lesion were visualized accurately (Fig. 3a) as determined by comparison to an anatomical photograph (Fig. 3b). The contrast in optical absorption ranged from 1.7 to 5.2.

The spatial resolution of our current PAT system was measured at  $\sim 0.2$  mm with the line-spread function of a tissue-equivalent phantom. The vessels in the cortical surface that can be visualized by PAT are between 0.04 mm and 0.36 mm in diameter as measured in the photograph, and therefore appear blurry owing to the 0.2-mm resolution of the PAT image. This resolution approaches the diffraction limit of the detected photoacoustic waves, indicating that the resolution of PAT is limited by the bandwidth of the detected photoacoustic signals, rather than by optical diffusion as is the case for pure optical imaging.

### Functional imaging of cortex during whisker stimulation

We also used our PAT system to visualize the functional representations of whiskers in the cerebral cortex of rats. During functional imaging of cortical neural activities in response to whisker stimulation, the temperature of the water in the tank was maintained approximately at the body temperature of the rat. Stimulating the

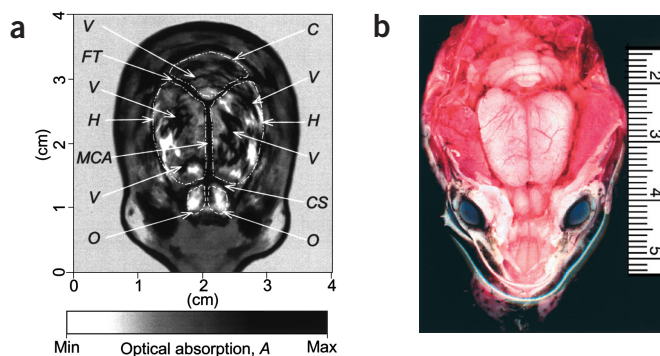


**Figure 2** PAT imaging of the rat brain *in vivo*. (a) Noninvasive PAT image of the superficial layer of a rat brain acquired with the skin and skull intact, with optical absorption shown in grayscale (darker areas indicate greater absorption). C, cerebellum; H, cerebral hemispheres; O, olfactory bulbs; MCA, middle cerebral artery; CS, cruciate sulcus; FT, fissura transversa; V, blood vessels. The matrix size of the image was 1,000 (horizontal)  $\times$  1,000 (vertical), showing a 4 cm  $\times$  4 cm region. The blood vessels distributed in the superficial layer of the cerebrum and cerebellum are clearly visible with high optical contrast and accurate localization. (b) Open-skull photograph of the rat brain surface acquired after the PAT experiment.

left and right whiskers, respectively, we obtained two PAT images of the rat superficial cortex. Subtracting the PAT image without whisker stimulation from the two PAT images with whisker stimulation produced two maps of functions evoked by these stimuli.

We successfully imaged functional cerebral hemodynamic changes in response to whisker stimulation on either side of the rat snout. Vascular patterns in the activated regions (Fig. 4a) matched the imaged distributions of functional signals well (Fig. 4b,c), indicating that the functional signals detected here by PAT resulted from hemodynamic changes in the large blood vessels in the superficial cortex. The activated regions visualized by PAT are marked on the photograph of the brain cortical surface by two dotted frames (Fig. 4d). Because the activated region lies in the hemisphere corresponding to opposite-side whisker stimulation, the observed changes in photoacoustic signals are believed to be induced by whisker activity. The rat recovered normally after imaging, and a histological evaluation was then made of its cerebral cortex. The vibrotome sections of cortical layer IV of the specialized region of the rat cerebral cortex—termed the whisker-barrel cortex (Fig. 4e)—colocalize well with the activated regions in the functional PAT images.

### DISCUSSION

It is widely accepted that increases in neural activity are accompanied by increases in local cerebral blood flow and regional metabolic activity in the homonymous activated region<sup>11,12,24</sup>. The PAT system enables us, by noninvasive means, to localize the hemodynamic responses clearly and accurately to neural activities and metabolic increases as a consequence of whisker stimulation. The detected differential optical absorption results from a complex interplay of blood volume, blood flow and oxygen consumption. Because deoxy- and oxyhemoglobin have similar extinction coefficients at 532 nm, the dominant factor that intensifies the photoacoustic signals is believed to be an increase in vascular blood volume (or flow) in the activated region around the whisker-barrel cortex during stimulation. The observed fractional change in optical absorption,  $\Delta A/A$ , in the large blood vessels within the activated regions was up to 8%. The functional PAT images are characterized

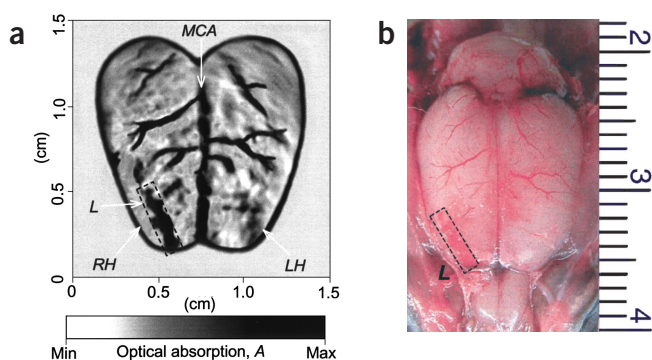


**Figure 3** PAT imaging of the rat brain lesion *in situ*. (a) Noninvasive PAT image of a superficial lesion (1 mm × 4 mm, in the right cortex cerebri—area frontalis) on a rat's cerebra acquired with the skin and skull intact. RH, right cerebral hemisphere; LH, left cerebral hemisphere; L, lesion. The blood vessels distributed on both sides of the middle cerebral artery (MCA) are imaged clearly. The matrix size of the image was 1,000 (horizontal) × 1,000 (vertical), showing a 1.5 cm × 1.5 cm region. (b) Open-skull photograph of the rat cerebral surface acquired after the PAT experiment.

by a strong vascular pattern, which is believed to result from an increased inflow of fresh blood<sup>25,26</sup>. The areas of vascular response are clearly wider than the whisker-barrel cortex regions, as hemodynamic changes propagate through the feeding vessels and even spread to neighboring vessels.

This work demonstrated that PAT is a noninvasive means for localizing and quantifying regional brain hemodynamic responses to neural activities through the skin and skull with high optical contrast and high ultrasonic resolution *in vivo*. As a further demonstration of the ability to image global responses using PAT, we studied the systemic effects of hyperoxia and hypoxia. We obtained a functional image of vascular responses in the rat cerebral cortex to the alteration of inspired gas from 100% O<sub>2</sub> to hypoxic gas (5% O<sub>2</sub>, 5% CO<sub>2</sub> and 90% N<sub>2</sub>; see **Supplementary Fig. 1** online). Our findings indicated that changing from hyperoxia to hypoxia induces a significant increase in cerebral blood volume (or flow), in agreement with previous studies<sup>27–30</sup>. We have also obtained PAT images of the deep brain in small animals (see **Supplementary Fig. 2** online).

Because the current PAT system involves scanning using a single-element ultrasonic transducer, its temporal resolution is not high. At each scanning position, photoacoustic signal detection and averaging takes 4 s. For a 2 $\pi$  angular scan with a step size of 1.5°, the image acquisition time is ~16 min. In future, however, with the use of an ultrasonic transducer array and a laser system with a higher repetition rate, it should be possible to use PAT for real-time imaging.

Because the brain is highly responsive to changes in blood oxygenation, the applications of PAT will be greatly broadened when multiple wavelengths are used to achieve oxygen-dependent imaging with high temporal and spatial resolution<sup>31–33</sup>. PAT should be able to visualize brain neoplasias and brain metastases from distant organs. In addition, in combination with reporter genes, PAT offers promise for imaging pathologic processes at molecular genetic levels, monitoring the delivery of vectors to specific cells in gene therapy, and visualizing the magnitude and retention of therapeutic gene expression. All of these goals can be accomplished by virtue of the technique's high optical contrast and ultrasonic diffraction-limited spatial resolution. PAT imaging of the human brain, although more difficult, is also feasible.

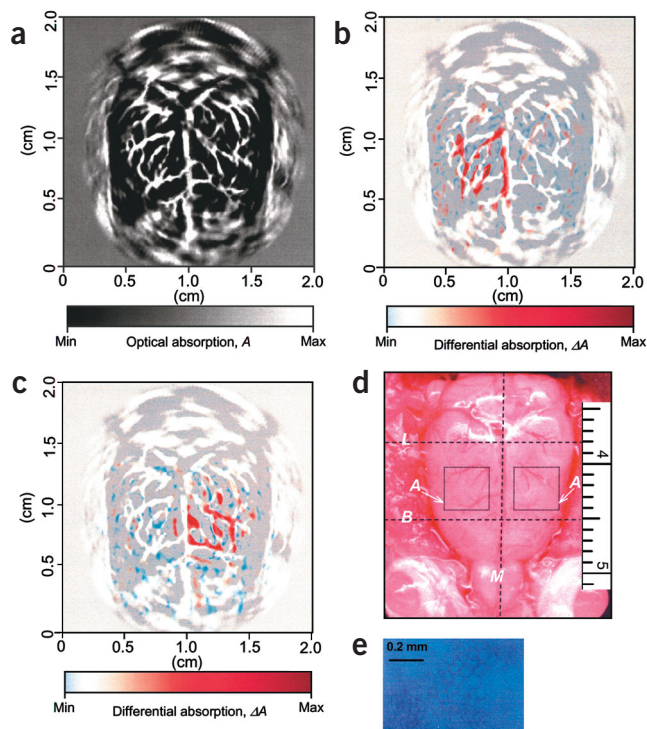


**Figure 4** Functional imaging of cerebral hemodynamic changes in response to whisker stimulation. (a) Noninvasive PAT image of the vascular pattern in the superficial layer of the rat cortex acquired with the skin and skull intact. The matrix size of the image was 1,000 (horizontal) × 1,000 (vertical), showing a 2.0 cm × 2.0 cm region. (b,c) Noninvasive functional PAT images corresponding to left-side and right-side whisker stimulation, respectively, acquired with the skin and skull intact. These two maps of functional representations of whiskers are superimposed on the image of the vascular pattern in the superficial cortex shown in a. (d) Open-skull photograph of the rat cortical surface. B, bregma; L, lambda; M, midline; A, activated regions corresponding to whisker stimulation (4 mm × 4 mm). (e) Histology of normal lamina IV cortical barrels, located in regions A, representing the large mystacial vibrissae of the rat somatosensory system (40× magnification).

## METHODS

**Experimental rats.** The brains of adult Sprague-Dawley rats (Charles River Breeding Laboratories, ~350 g) were imaged by PAT. Before imaging, the hair on each rat's head was removed with hair remover lotion. A dose of 87 mg/kg ketamine plus 13 mg/kg xylazine, administered intramuscularly, was used to briefly anesthetize the rats, and supplemental injections of a similar anesthetic mixture (~10 mg/kg/h) kept the rats motionless throughout the experiment. The mouths and noses of the rats were covered with an aerophore to allow them to breathe in the water. Average thicknesses of the skin and the skull covering the brain were about 0.6 and 0.8 mm, respectively. Laser light penetrated through the skin and the skull (which homogenized the incoming light further by scattering) to the rat brain. After the data acquisition for PAT, rats were killed using pentobarbital (120 mg/kg, administered intraperitoneally (i.p.)). Subsequently, an open-skull anatomical photograph of the brain surface was taken as a control.

**Induction of brain lesions.** Each rat was deeply anesthetized with pentobarbital (100 mg/kg, i.p.) and the surface of the head was disinfected with alcohol swabs (70% isopropyl alcohol). A sterile, curved (90° angle) syringe needle (22 G × 1 inch) was inserted through the skin and skull bone on the right cortex cerebri to induce a superficial cortical lesion. The rat's brain was imaged immediately by PAT. Then, for comparison, an open-skull photograph of the cerebral cortex was taken.

**Whisker stimulation.** For the initial experiments, to obtain the strongest functional signals correlated with the whisker stimulation, all whiskers on one side

of the snout were deflected simultaneously with a relay driven by a computer-controlled function generator. The whiskers were deflected at 10 Hz with an oscillation amplitude of ~8 mm at a distance of ~10 mm from the whisker pad. At each scanning position, whisker stimulation was maintained for 4.5 s and the photoacoustic signal was collected during the 0.5–4.5 s after the start of whisker stimulation.

**Histology.** Each rat, under anesthesia (100 mg/kg pentobarbital, i.p.), was perfused with buffered 4% formaldehyde via the left heart ventricle, and the brain cortex was isolated and flattened between glass slides to a thickness of 2 mm. The isolated cortex was cut tangentially with a vibrotome to the pia mater at a thickness of 60  $\mu$ m. Vibrotome sections were collected in a multiwell Costar dish in 0.1 M phosphate-buffered saline, pH 7.4. The cortical barrels<sup>34</sup> in layer IV, found 500  $\mu$ m below the cortical surface, were photographed with an inverted Olympus microscope at a 40 $\times$  magnification.

**Ethical review of procedures.** All experimental animal procedures were performed in conformity with the guidelines of the US National Institutes of Health<sup>35</sup>. The laboratory animal protocol for this work was approved by the ULAC of Texas A&M University, College Station, Texas, USA.

Note: Supplementary information is available on the Nature Biotechnology website.

#### ACKNOWLEDGMENTS

This research was supported in part by the US Department of Defense, National Institutes of Health, National Science Foundation, and Texas Advanced Research Program.

#### COMPETING INTERESTS STATEMENT

The authors declare that they have no competing financial interests.

Received 20 November 2002; accepted 7 April 2003

Published online 15 June 2003; doi:10.1038/nbt839

- Grinvald, A., Frostig, R.D., Lieke, E. & Hildesheim, R. Optical imaging of neuronal activity. *Physiol. Rev.* **68**, 1285–1365 (1988).
- Frostig, R.D., Lieke, E.E., Ts'o, D.Y. & Grinvald, A. Cortical functional architecture and local coupling between neuronal activity and the microcirculation revealed by *in vivo* high resolution optical imaging of intrinsic signals. *Proc. Natl. Acad. Sci. USA* **87**, 6082–6086 (1990).
- MacVicar, B.A. & Hochman, D. Imaging of synaptically evoked intrinsic optical signals in hippocampal slices. *J. Neurosci.* **11**, 1458–1469 (1991).
- Ebner, T.J. & Chen, G. Use of voltage-sensitive dyes and optical recordings in the central nervous system. *Prog. Neurobiol.* **46**, 463–506 (1995).
- Villringer, A. & Chance, B. Non-invasive optical spectroscopy and imaging of human brain function. *Trends. Neurosci.* **20**, 435–442 (1997).
- Mayhew, J. *et al.* Spectroscopic analysis of changes in remitted illumination: the response to increased neural activity in brain. *Neuroimage* **10**, 304–326 (1999).
- Nemoto, M. *et al.* Analysis of optical signals evoked by peripheral nerve stimulation in rat somatosensory cortex: dynamic changes in hemoglobin concentration and oxygenation. *J. Cereb. Blood Flow Metab.* **19**, 246–259 (1999).
- Gratton, G. & Fabiani, M. Dynamic brain imaging: event-related optical signals (EROS) measures of the time course and localization of cognitive-related activity. *Psychon. Bull. Rev.* **5**, 535–563 (1998).
- Grinvald, A., Lieke, E., Frostig, R.D., Gilbert, C.D. & Wiesel, T.N. Functional architecture of cortex revealed by optical imaging of intrinsic signals. *Nature* **324**, 361–364 (1986).
- Haglund, M.M., Ojemann, G.A. & Hochman, D.W. Optical imaging of epileptiform and functional activity in human cerebral cortex. *Nature* **358**, 668–671 (1992).
- Dowling, J.L., Henegar, M.M., Liu, D., Rovainen, C.M. & Woolsey, T.A. Rapid optical imaging of whisker responses in the rat barrel cortex. *J. Neurosci. Meth.* **66**, 113–122 (1996).
- Jones, M., Berwick, J. & Mayhew, J. Changes in blood flow, oxygenation, and volume following extended stimulation of rodent barrel cortex. *Neuroimage* **15**, 474–487 (2002).
- Hoelen, C.G.A., de Mul, F.F.M., Pongers, R. & Dekker, A. Three-dimensional photoacoustic imaging of blood vessels in tissue. *Opt. Lett.* **23**, 648–650 (1998).
- Kruger, R.A., Reinecke, D.R. & Kruger, G.A. Thermoacoustic computed tomography—technical considerations. *Med. Phys.* **26**, 1832–1837 (1999).
- Esenaliev, R.O., Karabutov, A.A. & Oraevsky, A.A. Sensitivity of laser photoacoustic imaging in detection of small deeply embedded tumors. *IEEE J. Sel. Top. Quant.* **5**, 981–988 (1999).
- Paltauf, G. & Schmidt-Kloiber, H. Optical method for two-dimensional ultrasonic detection. *Appl. Phys. Lett.* **75**, 1048–1050 (1999).
- Karabutov, A.A., Savateeva, E. & Podymova, N.B. Backward mode detection of laser-induced wide-band ultrasonic transients with photoacoustic transducer. *J. Appl. Phys.* **87**, 2003–2014 (2000).
- Köstli, K.P. *et al.* Photoacoustic imaging using a three-dimensional reconstruction algorithm. *IEEE J. Sel. Top. Quant.* **7**, 918–923 (2001).
- Wang, X. *et al.* Photoacoustic tomography of biological tissues with high cross-section resolution: reconstruction and experiment. *Med. Phys.* **29**, 2799–2805 (2002).
- Tokuno, H., Hatanaka, N., Takada, M. & Nambu, A. B-mode and color Doppler ultrasound imaging for localization of microelectrode in monkey brain. *Neurosci. Res.* **36**, 335–338 (2000).
- Diebold, G.J., Sun, T. & Khan, M.I. in *Photoacoustic and Photothermal Phenomena III* (ed. Bicanic, D.) 263–296 (Springer, Berlin, Heidelberg, 1992).
- Sun, T. & Diebold, G.J. Generation of ultrasonic waves from a layered photoacoustic source. *Nature* **355**, 806–808 (1992).
- Xu, M. & Wang, L.V. Time-domain reconstruction for thermoacoustic tomography in a spherical geometry. *IEEE T. Med. Imaging* **21**, 814–822 (2002).
- Gerrits, R.J., Stein, E.A. & Greene, A.S. Blood flow increases linearly in rat somatosensory cortex with increased whisker movement frequency. *Brain Res.* **783**, 151–157 (1998).
- Ogawa, S. *et al.* Intrinsic signal changes accompanying sensory stimulation: functional brain mapping with magnetic resonance imaging. *Proc. Nat. Acad. Sci. USA* **89**, 5951–5955 (1992).
- Hoge, R.D. *et al.* Investigation of BOLD signal dependence on cerebral blood flow and oxygen consumption: the deoxyhemoglobin dilution model. *Magn. Reson. Med.* **42**, 849–863 (1999).
- Kety, S.S. & Schmidt, C.F. The effects of altered arterial tensions of carbon dioxide and oxygen on cerebral blood flow and cerebral oxygen consumption of normal young men. *J. Clin. Invest.* **27**, 484–491 (1948).
- Siesjo, B. *Brain Energy Metabolism* (John Wiley, New York, 1978).
- Bereczki, D. *et al.* Hypoxia increases velocity of blood-flow through parenchymal microvascular systems in rat brain. *Cerebr. Blood F. Met.* **13**, 475–486 (1993).
- Duong, T.Q., Iadecola, C. & Kim, S.G. Effect of hyperoxia, hypercapnia, and hypoxia on cerebral interstitial oxygen tension and cerebral blood flow. *Magn. Reson. Med.* **45**, 61–70 (2001).
- Millikan, G.A. The oximeter, an instrument for measuring continuously the oxygen saturation of arterial blood in man. *Rev. Sci. Instrum.* **13**, 434–444 (1942).
- Jöbsis, F.F. Noninvasive, infrared monitoring of cerebral and myocardial oxygen sufficiency and circulatory parameters. *Science* **198**, 1264–1267 (1977).
- Mayevsky, A. & Chance, B. Intracellular oxidation-reduction state measured *in situ* by a multichannel fiberoptic surface fluorometer. *Science* **217**, 537–540 (1982).
- Vanderlo, H. & Woolsey, T.A. Somatosensory cortex-structural alterations following early injury to sense organs. *Science* **179**, 395–398 (1973).
- US National Institutes of Health. *Guide for the Care and Use of Laboratory Animals, NIH Publication No. 86-23* (US Government Printing Office, Washington, DC, USA, 1985).